Asymmetric Distribution of Lunar Impact Basins Caused by Variations in Target Properties

Katarina Miljković[1*], Mark A. Wieczorek[1], Gareth S. Collins[2], Matthieu Laneuville[1], Gregory A. Neumann[3], H. Jay Melosh[4], Sean C. Solomon[5,6], Roger J. Phillips[7], David E. Smith[8] and Maria T. Zuber[8]

[1]Institut de Physique du Globe de Paris, Sorbonne Paris Cité, Université Paris Diderot, Case 7011, Lamarck A, 5, 35 rue Hélène Brion, 75205 Paris Cedex 13, France.

[2]Department of Earth Sciences and Engineering, Imperial College London, South Kensington Campus, SW7 2AZ, London, UK.

[3]Solar System Exploration Division, NASA Goddard Space Flight Center, Greenbelt, MD 20771, USA.

[4]Department of Earth, Atmospheric, and Planetary Sciences, Purdue University, 550 Stadium Mall Drive, West Lafayette, IN 47907, USA.

[5]Department of Terrestrial Magnetism, Carnegie Institution of Washington, Washington, DC 20015, USA.

[6]Lamont-Doherty Earth Observatory, Columbia University, Palisades, NY 10964, USA.

[7]Planetary Science Directorate, Southwest Research Institute, Boulder, CO 80302, USA.

[8] Department of Earth, Atmospheric and Planetary Sciences, Massachusetts Institute of Technology, Cambridge, MA 02139-4307, USA.

[*]To whom correspondence should be addressed; E-mail: miljkovic@ipgp.fr

Maps of crustal thickness derived from NASA's Gravity Recovery and Interior Laboratory (GRAIL) mission revealed more large impact basins on the nearside hemisphere of the Moon than on its farside. The enrichment in heat-producing elements and prolonged volcanic activity on the lunar nearside hemisphere indicate that the temperature of the nearside crust and upper mantle was hotter than that of the farside at the time of basin formation. Using the iSALE-2D hydrocode to model impact basin formation, we found that impacts on the hotter nearside would have formed basins up to two times larger than similar impacts on the cooler farside hemisphere. The size distribution of lunar impact basins is thus not representative of the earliest inner Solar system impact bombardment.

Progress in understanding impact basins on the Moon has been hampered by the simple fact that there is a lack of consensus on the size of the largest basins (*1–3*). From an impact physics perspective, the most relevant metric for the size of a basin is the diameter of its transient cavity, but as its name implies, this structure is short-lived and its diameter is not easily estimated from surface measurements (*4*). Most impact basins on the nearside hemisphere of the Moon have been filled by lava flows, hiding important morphological clues that could be used for determining the size of the transient cavity. Other impact basins have multiple rings, and it is unclear which of these, if any, most closely approximates the transient cavity. Because the impact process excavates large quantities of crustal material and uplifts mantle material beneath the basin center, an alternative metric for the size of a basin is the diameter of the region of crustal thinning (*5–7*). High-resolution gravity data obtained from NASA's Gravity Recovery and Interior Laboratory (GRAIL) mission (*8*) have provided global maps of crustal thickness on the Moon (*9*) that allow for an unambiguous determination of the region of crustal thinning for all impact basins greater than 200 km diameter.

GRAIL gravity data show that lateral variations in the Moon's crustal thickness are dominated by impact basins ranging in diameter from about 200 to 2000 km (*9*). Approximately half of those basins formed in the Imbrian and Nectarian periods from about 3.7 to perhaps 4.2 Ga (billion years ago) (*10, 11*) (Table S1). The sole exception is the South Pole-Aitken basin, which is the oldest and largest impact structure on the Moon, and which we do not consider further on the grounds that it likely formed during a much earlier epoch than the other basins for which variations in crustal thickness have been preserved. We quantify the size of lunar impact basins by the diameter D of the region of crustal thinning (*1*). There are 12 basins on each hemisphere with diameters greater than 200 km and crust thinned to a few kilometers, resolved by GRAIL (Fig. 1). Although the total number of basins is equal on the two hemispheres, their size distribution is highly asymmetric (Fig. 2). Whereas there are eight basins on the nearside hemisphere with diameters greater than 320 km, only one of this size is found on the farside, and this basin (Orientale, 94° W, 20° S) straddles the western limb of the Moon. Simulations of the Moon's impact bombardment by near-Earth asteroids show that the difference in cratering rate between the nearside and farside hemispheres should be less than 1% (*12*) for a large range of impact conditions. With a uniform cratering rate, there is less than 2% probability that eight basins greater than 320 km diameter would form on the nearside and only one on the farside (Fig. S1).

The Moon shows major geological differences between the nearside and farside hemispheres. The nearside is dominated by the compositionally unique Procellarum KREEP Terrane (PKT), which is highly enriched in heat-producing and other incompatible elements that likely formed during the late stages of magma-ocean crystallization (*13,14*) (Fig. 1). Over 99% by area of the Moon's exposed basaltic lavas erupted on the lunar nearside, a concentration attributed to higher than average nearside mantle temperatures, at least in part the result of the high concentration of heat-producing elements in the nearside crust and upper mantle (*15*). The evidence

for viscous relaxation of topographic relief of nearside basins (*16, 17*) and the presence of mare basalts extending beyond the confines of the surface area of thorium enrichment (that defines the PKT) suggest that higher than average subsurface temperatures surrounded the PKT for a considerable interval of lunar history. Several models have been proposed to account for the hemispheric differences in volcanic activity and heat-producing elements, all of which predict hemispheric differences in crustal and upper mantle temperatures (*15, 18–20*). We propose that hemispheric differences in subsurface temperature and, to a lesser extent, crustal thickness (*9*) are the cause of the asymmetric distribution of large impact basins. We tested this hypothesis using numerical simulations of impact basin formation.

To investigate the consequences of impact basin formation on the two lunar hemispheres we used the iSALE-2D shock-physics hydrocode (*21–23*). Vertical impacts onto the lunar surface were modeled with impact speeds of 10 and 17 km s^{-1}. From available material models and following previous work (*24, 25*), we used basalt and dunite to represent the lunar crust and mantle, respectively, and dunite to represent the impactor (Table S2). The pre-impact crustal thickness for the nearside and farside was set to 30 and 60 km, respectively. Representative subsurface temperature profiles beneath the nearside PKT and the farside hemisphere during the basin-forming epoch 4 Ga were obtained from a three-dimentional thermo-chemical convection code (*26*) that included the asymmetric heat-source distribution associated with the PKT (*20*) and provided results similar to those of previous asymmetric models (*15*) (Fig. S2). For a given impact velocity and impactor diameter, six impact simulations were performed, each with different temperature profiles for each hemisphere (Tables S3, S4).

Our simulations show that lunar impact basins form via the growth of a deep, bowl-shaped transient cavity that is gravitationally unstable and that collapses by a combination of uplift of the crater floor and inward collapse of the crater rim (*7, 25*). The crustal structure is modified in several ways during this process (Fig. S4). During the formation of the transient crater, crustal

material is ejected from inside the transient crater rim and deposited outside the transient crater; this process thins the crust inside the crater rim and thickens it outside (Fig. S4). Because the size of the transient crater is limited by the impact energy available to displace the excavated mass in the ambient gravity field, the diameter of crustal thinning at this intermediate stage depends primarily on the impactor mass and speed and only weakly on the ambient temperature or crustal thickness. However, the subsequent collapse of the transient crater, and the consequent modifications in crustal structure, depend sensitively on the shear strength of the crust and upper mantle, which is a strong function of temperature. On the cooler and stronger farside, as mantle beneath the crater floor is uplifted, crust beneath the transient crater rim collapses inwards, forming a collar of crust around the mantle uplift and resulting in a diameter of thinned crust that is smaller than the transient crater diameter. In contrast, the collapse of the transient crater on the warmer and weaker nearside is more extensive: the mantle below the crater floor is uplifted farther and over a much broader region, which prevents the thickened crust surrounding the transient crater from collapsing back into the crater. As a result, the diameter of crustal thinning is substantially larger on the hot nearside than on the cold farside (Fig. 3).

The diameter of crustal thinning for a lunar basin formed in the nearside thin crust is plotted in Fig. 4 as a function of the diameter that would occur for the same impact in the farside thick crust. The crustal thinning diameter does not differ markedly between the two hemispheres when the same temperature profile is used. Nevertheless, as demonstrated by crustal thickness profiles in Fig. 3, the ambient crustal thickness does have an influence on the character of the final crustal thickness profile. In contrast, for the same impact conditions, the crustal thinning diameter is greatly affected by temperature profile. Despite forming a nearly identical transient cavity, nearside basins formed in a hot target can have diameters of thinned crust up to two times larger than the respective farside basins formed under similar conditions but in cold crust. These relationships between the diameter of crustal thinning on the nearside and farside hemispheres

are largely independent of impact speed (from 10 km/s to 17 km/s) and do not depend on differences in time of basin formation of up to a few hundred million years (Fig. S3, Table S4, Eqs. S4–S7).

The empirical relations from Fig. 4 can be used to compensate for the increase in basin size that results from lateral variations in target properties. Given that the absolute ages of most large lunar basins are poorly known, and that the subsurface temperature profile will vary both with time and distance from the PKT, such an exercise will be somewhat qualitative. We assumed that basins located within the PKT formed in the hottest and thinnest crust, and that basins surrounding the PKT formed in crust of intermediate temperature and thickness, and we then corrected the sizes of these basins to those that would be expected for impacts into the temperature regime of the colder farside highlands (Section S5). Once lateral variations in target properties are included, Fig. 2 shows that the size distributions of impact basins on the nearside and farside hemispheres are comparable.

The concept of the late heavy bombardment (a spike in the impact cratering rate about 4 Ga) (*27–29*) is based largely on the nearside impact basins that are either within, or adjacent to, the Procellarum KREEP Terrane. The temperature profile beneath this region is not representative of the Moon as a whole, and the special nature of the lunar nearside implies that the magnitude of basin-forming impact bombardment has been overestimated, mainly in terms of the impactor mass flux. The size distribution of impact basins on the farside hemisphere of the Moon is a more accurate indicator of the impact history of the inner solar system than that on the nearside. Lateral variations in target properties could have affected the size distribution of impact basins on other planets, such as Mars, which possesses a marked dichotomy in crustal thickness between the northern lowlands and southern highlands. A different temperature profile, combined with lateral variations in crustal temperature (*30*), could be responsible for the lower density of large impact basins on Mercury (*31*) than on the Moon, and higher surface

temperatures are likely to have played an important role in determining the final sizes of craters on Venus.

References and Notes

1. Wieczorek, M. A., Phillips, R. J. Lunar multiring basins and the cratering process. *Icarus* **139**, 246–259 (1999).

2. Hikida, H., Wieczorek, M. A. Crustal thickness of the Moon: New constraints from gravity inversions using polyhedral shape models. *Icarus* **192**, 150–166 (2007).

3. Fassett, C. I. *et al.* Lunar impact basins: Stratigraphy, sequence and ages from superposed impact crater populations measured from Lunar Orbiter Laser Altimeter (LOLA) data. *J. Geophys. Res.* **117**, E00H06 (2012).

4. Turtle, E. P. *et al.* Impact structures: What does crater diameter mean? In *Large Meteorite Impacts III* (eds. Kenkmann, T., Hörz, F., Deutsch, A.), pp. 1–24, Spec. Paper 384 (Geological Society of America, Boulder, Colo., 2005).

5. Neumann, G. A., Zuber, M. T., Smith, D. E., Lemoine, F. G. The lunar crust: Global structure and signature of major basins. *J. Geophys. Res.* **101**, 16,841–16,863 (1996).

6. Bratt, S. R., Solomon, S. C., Head, J. W., Thurber, C. H. The deep structure of lunar basins: Implications for basin formation and modification. *J. Geophys. Res.* **90**, 3049–3064 (1985).

7. Potter, R., Kring, D. A., Collins, G. S., Kiefer, W., McGovern, P. Estimating transient crater size using the crustal annular bulge: Insights from numerical modeling of lunar basin-scale impacts. *Geophys. Res. Lett.* **39**, L18203 (2012).

8. Zuber, M. T. *et al.* Gravity field of the Moon from the Gravity Recovery and Interior Laboratory (GRAIL) mission. *Science* **339**, 668–671 (2013).

9. Wieczorek, M. A. *et al.* The crust of the Moon as seen by GRAIL. *Science* **339**, 671–675 (2013).

10. Norman, M. D., Duncan, R. A., Huard, J. J. Imbrium provenance for the Apollo 16 Descartes terrain: Argon ages and geochemistry of lunar breccias 67016 and 67455. *Geochim. Cosmochim. Acta* **74**, 763–783 (2010).

11. Fernandes, V. A., Fritz, J., Weiss, B. P., Garrick-Bethell, I., Shuster, D. L. The bombardment history of the Moon as recorded by ^{40}Ar–^{39}Ar chronology. *Meteorit. Planet. Sci.* **48**, 241–269 (2013).

12. Le Feuvre, M., Wieczorek, M. A. Nonuniform cratering of the Moon and a revised crater chronology of the inner Solar System. *Icarus* **214**, 1–20 (2011).

13. Jolliff, B. L., Gillis, J. J., Haskin, L. A., Korotev, R. L., Wieczorek, M. A. Major lunar crustal terranes: Surface expressions and crust-mantle origins. *J. Geophys. Res.* **105**, 4197–4216 (2000).

14. Korotev, R. L. The great lunar hot spot and the composition and origin of the Apollo mafic ("LKFM") impact-melt breccias. *J. Geophys. Res,* **105**, 4317–4346 (2000).

15. Wieczorek, M. A., Phillips, R. J. The "Procellarum KREEP Terrane": Implications for mare volcanism and lunar evolution. *J. Geophys. Res.* **105**, 20,417–20,430 (2000).

16. Solomon, S. C., Comer, R. P., Head, J. W. The evolution of impact basins: Viscous relaxation of topographic relief. *J. Geophys. Res.* **87**, 3975–3992 (1982).

17. Kamata, S. *et al.* Viscoelastic deformation of lunar impact basins: Implications for heterogeneity in the deep crustal paleo-thermal state and radioactive element concentration. *J. Geophys. Res.* **118**, 398–415 (2013).

18. Zhong, S., Parmentier, E. M., Zuber, M. T. A dynamic origin for the global asymmetry of lunar mare basalts. *Earth Planet. Sci. Lett.* **177**, 131–140 (2000).

19. Hess, P. C., Permentier, E. M. Thermal evolution of a thicker KREEP liquid layer. *J. Geophys. Res.* **106**, 28,023–28,032 (2001).

20. Laneuville, M., Wieczorek, M. A., Breuer, D., Tosi, N. Asymmetric thermal evolution of the Moon. *J. Geophys. Res.* **118**, 1435–1452 (2013).

21. Amsden, A. A., Ruppel, H. M., Hirt, C. W. SALE: A simplified ALE computer program for fluid flow at all speeds. **Report LA-8095**, 105 (Los Alamos National Laboratory, Los Alamos, New Mex., 1980).

22. Collins, G. S., Melosh, H. J., Ivanov, B. A. Modeling damage and deformation in impact simulations. *Meteorit. Planet. Sci.* **39**, 27–231 (2004).

23. Wünnemann, K. and Collins, G. S. and Melosh, H. J. A strain-based porosity model for use in hydrocode simulations of impacts and implications for transient-crater growth in porous targets. *Icarus* **180**, 514–527 (2006).

24. Pierazzo, E., Artemieva, N. A., Ivanov, B. A. Starting conditions for hydrothermal systems underneath Martian craters: Hydrocode modeling. In *Large Meteorite Impacts III* (eds. Kenkmann, T., Hörz, F., Deutsch, A.), pp. 443-457, Spec. paper **384**, (Geological Society of America, Boulder, Colo., 2005).

25. Ivanov, B. A., Melosh, H. J., Pierazzo, E. Basin-forming impacts: Reconnaissance modeling, In *Large Meteorite Impacts and Planetary Evolution IV* (eds. Gibson, R. L., Reimold, W. U.), pp. 29–49, Spec. paper **465**, (Geological Society of America, Boulder, Colo., 2010).

26. Hüttig, C., Stemmer, K. Finite volume discretization for dynamic viscosities on voronoi grids. *Phys. Earth Planet. Inter.* **171**, 137–146 (2008).

27. Tera, F., Papanastassiou, D. A., Wasserburg, G. J. Isotopic evidence for a terminal lunar cataclysm. *Earth Planet. Sci. Lett.* **22**, 1–21 (974).

28. Kring, D. A., Cohen, B. A. Cataclysmic bombardment throughout the inner solar system 3.9–4.0 Ga. *J. Geophys. Res.* **107**, 5009 (2002).

29. Tsiganis, K., Gomes, R., Morbidelli, A., Levison, H. F. Origin of the orbital architecture of the giant planets of the solar system. *Nature* **435**, 459–461 (2005).

30. Williams, J.-P., Ruiz, J., Rosenburg, M. A., Aharonson, O., Phillips, R. J., Insolation driven variations of Mercury's lithospheric strength, *J. Geophys. Res.* **116**, E01008 (2011).

31. Fassett, C. I. *et al.* Large impact basins on Mercury: Global distribution, characteristics, and modification history from MESSENGER orbital data. *J. Geophys. Res.* **117**, E00L08 (2012).

32. Lawrence, D. J. *et al.* Small-area thorium features on the lunar surface. *J. Geophys. Res.* **108**, 5102 (2003).

Acknowledgements: KM was funded by the UnivEarthS LabEx project of the University of Sorbonne Paris Cité (ANR-10-LABX-0023 and ANR-11-IDEX-0005-02). GSC was funded by STFC grant ST/J001260/1. Additional support for this work was provided by the French Space Agency (CNES). The GRAIL mission is supported by the Discovery Program of NASA and is

performed under contract to the Massachusetts Institute of Technology and the Jet Propulsion Laboratory, California Institute of Technology. We gratefully acknowledge the developers of iSALE-2D/3D (www.isale-code.de).

Supplementary Materials

www.sciencemag.org

Supplementary text

Figs. S1 – S4

Tables S1 – S5

References (33–54)

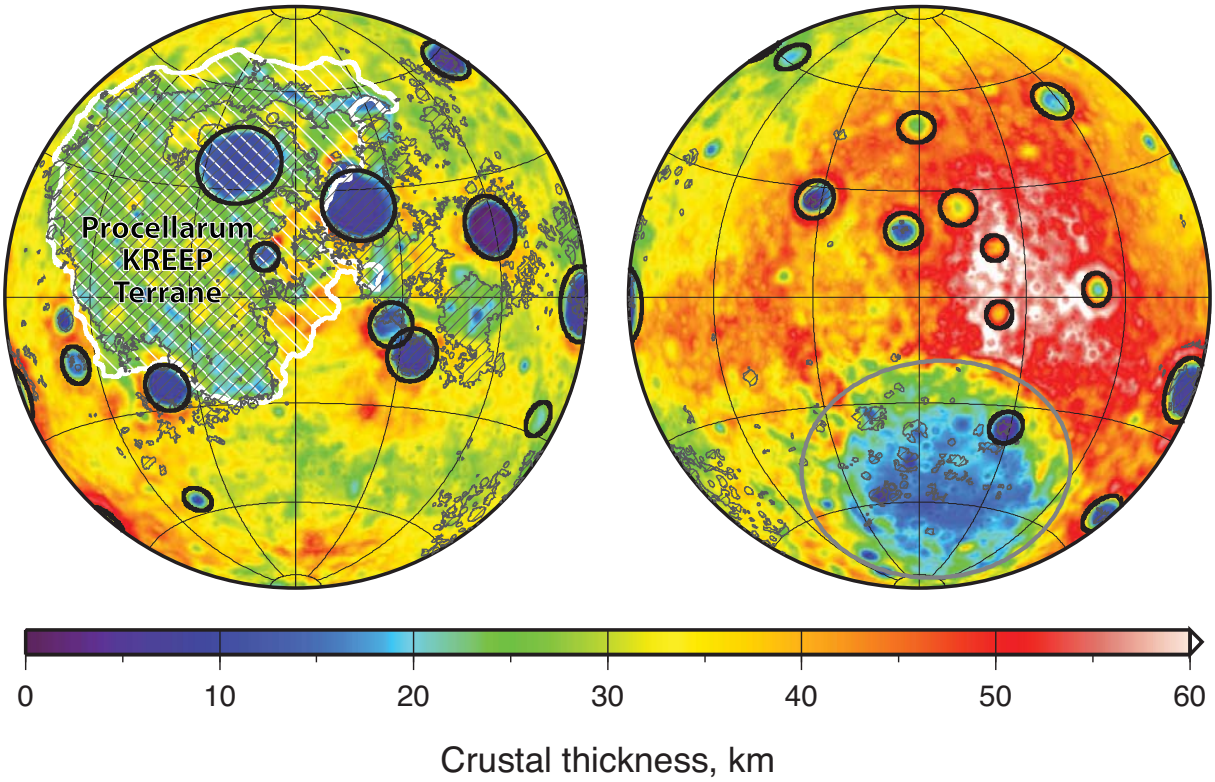

Fig. 1. Global map of crustal thickness on the Moon derived from GRAIL gravity data. Shown is the Procellarum KREEP Terrane (white cross ruling), defined by the 4 ppm contour of thorium (*32*), and the distribution of mare basalt (black cross ruling). Excluding the South Pole-Aitken basin (gray circle), there are 12 impact basins with diameters of crustal thinning greater than 200 km (black circles) on each hemisphere. This image is presented in two hemispherical Lambert azimuthal equal-area projections centered over the nearside (left) and farside (right) hemispheres.

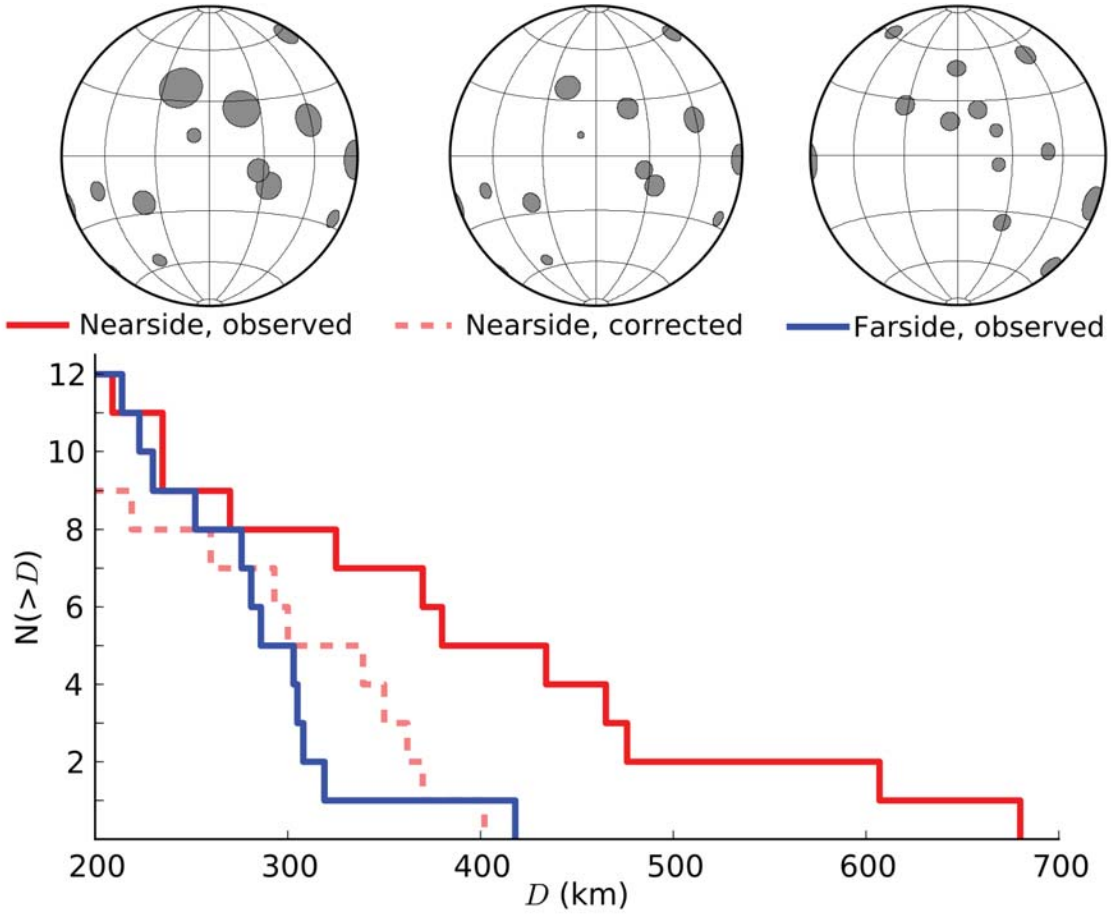

Fig. 2. Cumulative size distribution of observed lunar impact basins with diameters of crustal thinning D greater than 200 km for both hemispheres. The nearside is shown in solid red and farside in solid blue. The size distribution of nearside basins after correction for lateral variations in target properties is shown in dashed red. Hemispherical maps depict the sizes and locations of basins used in the size-frequency distributions.

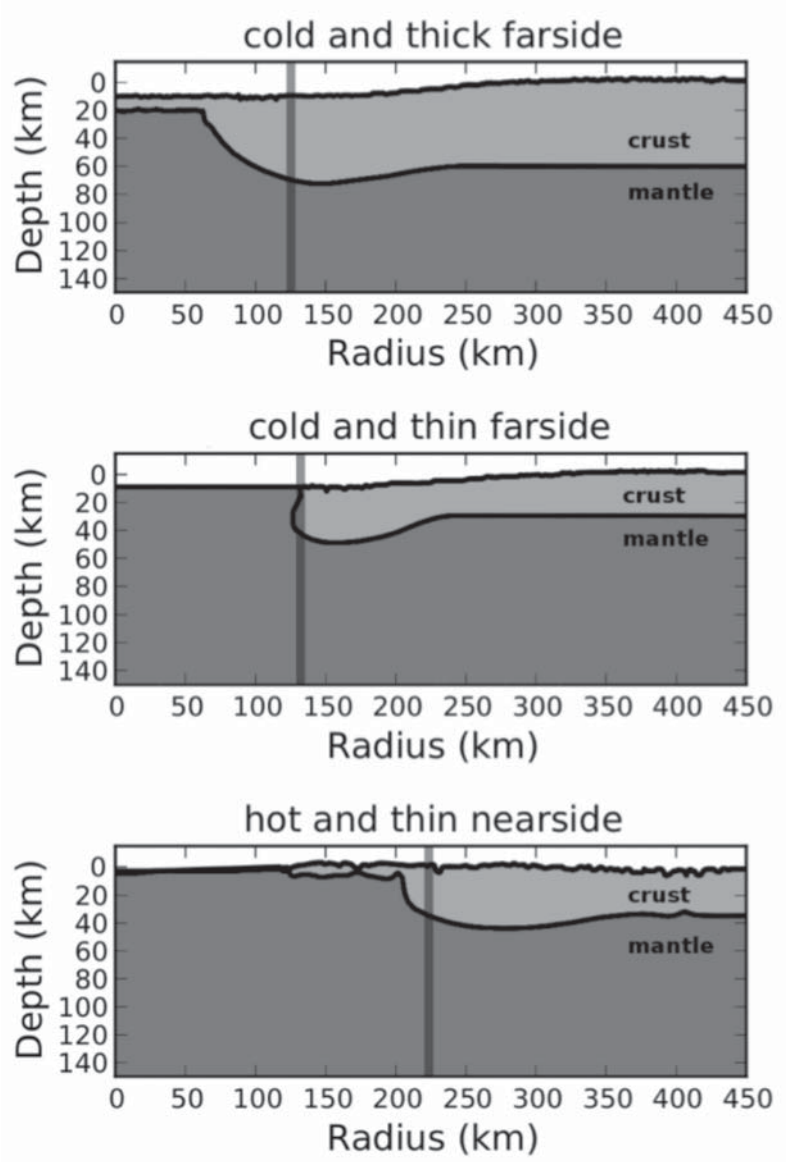

Fig. 3. Vertical cross-sections of final surface topography and depth of the crust-mantle interface for three simulations of lunar impact basin formation. Different temperature profiles for the farside (top and middle) and nearside (bottom) correspond to the lunar thermal state 4 Ga (M1/PKT1, Fig. S2). Pre-impact crustal thicknesses were 60 km (top) and 30 km (middle and bottom). The basins were formed by the vertical impact of a 45-km-diameter projectile at an impact speed of 17 km s^{-1} onto the Moon. The diameter of crustal thinning D shown by the vertical lines is the radial distance from basin center at which the crustal thickness reaches the pre-impact value.

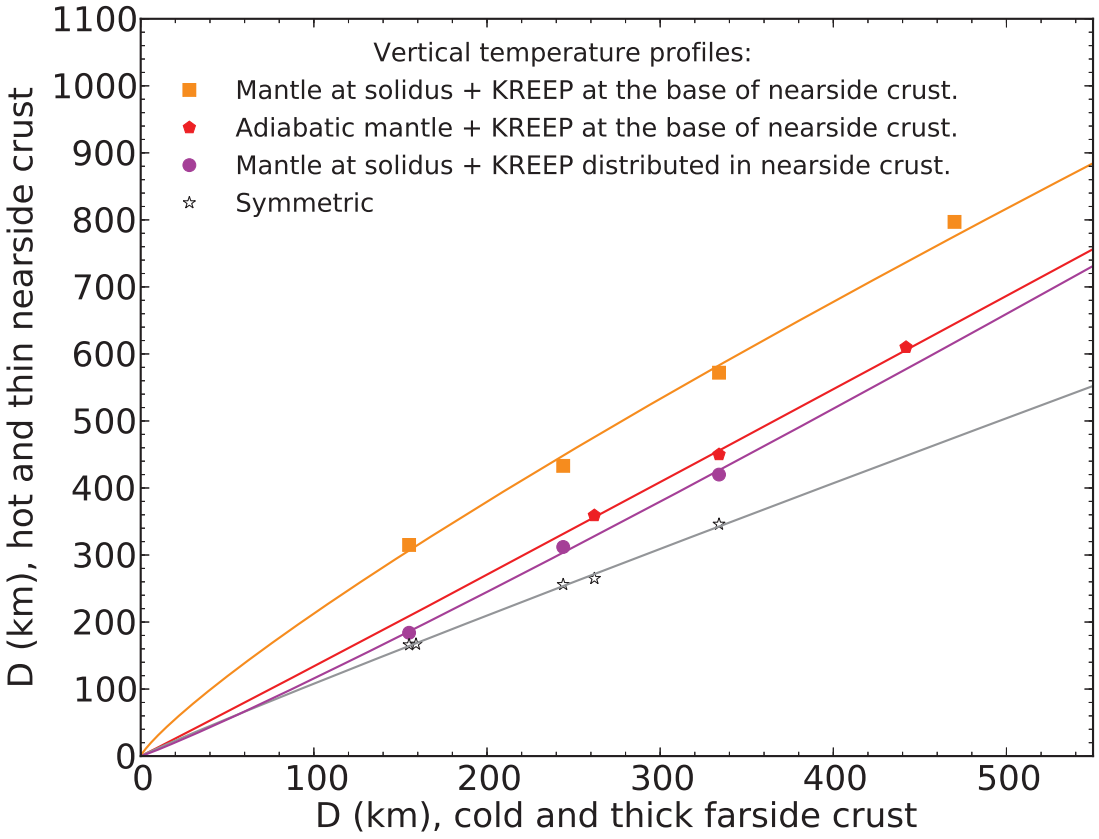

Fig. 4. Dependence of impact basin size on target properties. The abscissa is the diameter of crustal thinning D for a basin formed in a hot (KREEP-enriched) and 30-km-thick crust, and the ordinate is D for a basin formed in a cold and 60-km-thick crust, for the same size impactor. Points of the same color correspond to simulations with different projectile diameters. Variations for a given color reflect the different temperature profiles assumed for the nearside and farside: orange is for the hottest temperature profile for the nearside (M1/PKT1, Fig. S2) and violet is for the coolest (M1/PKT2, Fig. S2). Data in grey show D when the same temperature profile is used for both thin and thick crust.